J Gastroenterol
DOI 10.1007/s00535-009-0154-3

ORIGINAL ARTICLE—LIVER, PANCREAS, AND BILIARY TRACT

Hepatic senescence marker protein-30 is involved in the progression of nonalcoholic fatty liver disease

Hyohun Park · Akihito Ishigami · Toshihide Shima · Masayuki Mizuno · Naoki Maruyama · Kanji Yamaguchi · Hironori Mitsuyoshi · Masahito Minami · Kohichiroh Yasui · Yoshito Itoh · Toshikazu Yoshikawa · Michiaki Fukui · Goji Hasegawa · Naoto Nakamura · Mitsuhiro Ohta · Hiroshi Obayashi · Takeshi Okanoue

Received: 3 July 2009 / Accepted: 10 October 2009

Abstract
Background Both insulin resistance and increased oxidative stress in the liver are associated with the pathogenesis of nonalcoholic fatty liver disease (NAFLD). Senescence marker protein-30 (SMP30) was initially identified as a novel protein in the rat liver, and acts as an antioxidant and antiapoptotic protein. Our aim was to determine whether hepatic SMP30 levels are associated with the development and progression of NAFLD.
Methods Liver biopsies and blood samples were obtained from patients with an NAFLD activity score (NAS) ≤ 2 ($n = 18$), NAS of 3–4 ($n = 14$), and NAS ≥ 5 ($n = 66$).
Results Patients with NAS ≥ 5 had significantly lower hepatic SMP30 levels (12.5 ± 8.4 ng/mg protein) than patients with NAS ≤ 2 (30.5 ± 14.2 ng/mg protein) and patients with NAS = 3–4 (24.6 ± 12.2 ng/mg protein). Hepatic SMP30 decreased in a fibrosis stage-dependent manner. Hepatic SMP30 levels were correlated positively with the platelet count ($r = 0.291$) and negatively with the homeostasis model assessment of insulin resistance ($r = -0.298$), the net electronegative charge modified-low-density lipoprotein ($r = -0.442$), and type IV collagen 7S ($r = -0.350$). The immunostaining intensity levels of 4-hydroxynonenal in the liver were significantly and inversely correlated with hepatic SMP30 levels. Both serum large very low-density lipoprotein (VLDL) and very small low-density lipoprotein (LDL) levels in patients with NAS ≥ 5 were significantly higher than those seen in patients with NAS ≤ 2, and these lipoprotein fractions were significantly and inversely correlated with hepatic SMP30.
Conclusion These results suggest that hepatic SMP30 is closely associated with the pathogenesis of NAFLD, although it is not known whether decreased hepatic SMP30 is a result or a cause of cirrhosis.

Keywords SMP30 · NAFLD · NASH · Insulin resistance · Oxidative stress

H. Park · T. Shima · M. Mizuno · T. Okanoue (✉)
Department of Gastroenterology and Hepatology,
Saiseikai Suita Hospital, Kawazonocho 1-2,
Suita, Osaka 564-0013, Japan
e-mail: okanoue@suita.saiseikai.or.jp

A. Ishigami
Department of Biochemistry,
Faculty of Pharmaceutical Science,
Toho University, Chiba, Japan

A. Ishigami · N. Maruyama
Aging Regulation, Tokyo Metropolitan Institute
of Gerontology, Tokyo, Japan

H. Park · K. Yamaguchi · H. Mitsuyoshi · M. Minami ·
K. Yasui · Y. Itoh · T. Yoshikawa · T. Okanoue
Department of Molecular Gastroenterology and Hepatology,
Kyoto Prefectural University of Medicine,
Graduate School of Medical Science, Kyoto, Japan

M. Fukui · G. Hasegawa · N. Nakamura
Department of Endocrinology and Metabolism,
Kyoto Prefectural University of Medicine,
Graduate School of Medical Science, Kyoto, Japan

M. Ohta
Department of Medical Biochemistry,
Kobe Pharmaceutical University, Kobe, Japan

H. Obayashi
Institute of Bio-Response Informatics, Kyoto, Japan

Introduction

Nonalcoholic fatty liver disease (NAFLD) is one of the most common causes of chronic liver injury throughout the

Published online: 28 November 2009

world [1–3]. It represents a spectrum of conditions characterized histologically by macrovesicular hepatic steatosis, and the diagnosis is made in patients who have not consumed alcohol in amounts sufficient to be considered harmful to the liver.

NAFLD encompasses varying microscopic features that range from simple steatosis, which has a good prognosis, to nonalcoholic steatohepatitis (NASH), which has a poor prognosis. Liver biopsy is recommended as the gold standard for both the diagnosis and staging of fibrosis in patients with NASH [1, 4–6]. Hyperlipidemia, insulin resistance, and oxidative stress can contribute heavily to the initiation and progression of NAFLD [7–9]. However, the exact intricacies of the molecular and cellular mechanisms responsible for the progression from simple steatosis to NASH have not been fully elucidated.

Senescence marker protein-30 (SMP30), a 34-kDa protein originally identified in the rat liver, is a novel molecule that decreases in concentration with aging in an androgen-independent manner [10, 11]. SMP30 transcripts have been detected in a multitude of tissues, and its amino acid alignment reveals a highly conserved structure among humans, rats, and mice [11]. We have reported previously that SMP30 participates in Ca^{2+} efflux by activating the calmodulin-dependent Ca^{2+}-pump in HepG2 cells and renal tubular cells, conferring on these cells resistance to injury caused by high intracellular Ca^{2+} concentrations [12, 13]. Recently, we identified SMP30 as gluconolactonase (GNL), which is involved in L-ascorbic acid biosynthesis in mammals, although human beings are unable to synthesize vitamin C because there are many mutations in the gulonolactone oxidase gene, which catalyzes the conversion from L-gulono-γ-lactone to L-ascorbic acid [14]. To clarify whether a causal relationship exists between a decrease in SMP30/GNL levels and age-associated organ disorders, we established SMP30/GNL knockout (KO) mice [15]. The livers of SMP30/GNL KO mice are highly susceptible to tumor necrosis factor-α (TNF α) and Fas-mediated apoptosis [15]. In addition, they showed mitochondrial damage and abnormal accumulations of triglycerides, cholesterol, and phospholipids [16]. Furthermore, SMP30/GNL in brain and lung tissue appeared to have protective properties against oxidative stress associated with aging [17–20]. Because the SMP30/GNL KO mice showed changes in the liver that mimic the processes of NAFLD, we hypothesized that decreased levels of SMP30 may be linked to the pathogenesis of NAFLD. The purpose of this study was to investigate the role of SMP30 in the pathogenesis of NAFLD.

Patients and methods

Patients

The study protocol was approved by the ethics committee of Saiseikai Suita Hospital and Kyoto Prefectural University of Medicine, and informed consent was obtained from all subjects prior to their enrollment in the study. A total of 98 patients histologically diagnosed as having NAFLD at Saiseikai Suita Hospital or Kyoto Prefectural University Hospital between 2006 and 2008 were enrolled in this study.

All liver biopsy specimens were stained with hematoxylin–eosin and Masson's trichrome stains and examined by two experienced pathologists blinded to the patients' clinical or laboratory data or liver biopsy sequence. Patients with NAFLD were divided into the following groups: simple steatosis and mild NASH (stages 0–1), moderate NASH (stage 2), and advanced NASH (stage 3–4) according to the classification proposed by Brunt et al. [6]. Several liver tissues samples from these groups were embedded in Tissue-Tek OCT (Sakura Finetech, Tokyo, Japan) compound and stained with Oil Red O. The fibrosis staging system was classified as follows: stage 0, no fibrosis; stage 1, zone 3 predominant pericellular fibrosis; stage 2, zone 3 fibrosis plus periportal fibrosis; stage 3, bridging fibrosis; stage 4, cirrhosis. The grade of steatosis was defined as mild ($\leq$33%), moderate (34–65%), or advanced ($\geq$66%). In addition, the NAFLD activity score (NAS) system was used to classify NAFLD into "not NASH" (NAS $\leq$ 2), "borderline NASH" (NAS = 3–4), and "definite NASH" (NAS $\geq$ 5), as shown in Table 1, because the NAS system has been reported as a reliable scoring system for diagnosing NASH [5]. We excluded patients with alcohol intake exceeding 20 g/day and those who reported signs, symptoms, and/or a history of known liver disease including viral, genetic, autoimmune, and drug-induced liver disease, before evaluation of liver histology.

Immunohistochemistry

Liver biopsy specimens were preserved in 10% formalin and embedded in paraffin. Specimens were serially sectioned onto microscope slides at a thickness of 4 μm and then deparaffinized. After removal of paraffin, the liver sections were heated by microwaving in 0.1 M citrate buffer (pH 7.0), followed by inactivation of endogenous peroxidases by incubation with 1% hydrogen peroxide (H_2O_2) in methanol. The primary antibodies used were monoclonal antibody raised against recombinant human SMP30 (1:2000 dilution) [14] and anti-4-hydroxynoneral

Table 1 Clinical features and laboratory data of three patient groups classified according to NAS scores

	Group A ($n = 18$) NAS ≤ 2	Group B ($n = 14$) NAS 3–4	Group C ($n = 66$) NAS ≥ 5
Male/female	9/9	6/8	34/32
Age (years)	60.9 ± 13.1	53.3 ± 16.8	60.4 ± 12.2
Body mass index (kg/m^2)	26.4 ± 4.8	27.5 ± 4.4	27.5 ± 4.8
Systolic blood pressure (mmHg)	133 ± 18	137 ± 8	140 ± 18
Diastolic blood pressure (mmHg)	77 ± 9	84 ± 12	82 ± 12
HbA1c (%)	6.2 ± 1.6	6.4 ± 1.8	6.3 ± 1.3
Fasting glucose (mg/dL)	116 ± 32	125 ± 41	124 ± 44
Fasting insulin (μU/mL)	8.5 ± 4.9	10.9 ± 4.7	12.7 ± 7.6
HOMA-R	2.9 ± 1.7	3.7 ± 2.1	3.9 ± 2.8*
AST (U/L)	39 ± 12	43 ± 12	44 ± 23
ALT (U/L)	37 ± 11	41 ± 10	53 ± 25
Triglyceride (mg/dL)	160 ± 67	149 ± 72	165 ± 94
Total cholesterol (mg/dL)	221 ± 42	208 ± 36	202 ± 34
HDL cholesterol (mg/dL)	55 ± 22	50 ± 7	49 ± 12
LDL cholesterol (mg/dL)	134 ± 25	119 ± 28	129 ± 30
Oxidized LDL (U/ml)	13.3 ± 2.6	13.8 ± 1.1	14.8 ± 2.2
Electronegative charge modified-LDL (ecd)	3.1 ± 3.0	3.1 ± 3.2	6.4 ± 3.5*
Type IV collagen 7S (ng/dL)	3.9 ± 0.5	4.0 ± 1.2	5.7 ± 1.9*
Platelet count (× 10^4/μL)	21.9 ± 2.9	21.9 ± 4.5	17.1 ± 4.7*
SMP30 in liver tissue (ng/mg protein)	30.5 ± 14.2	24.6 ± 12.2	12.5 ± 8.4*****
75 g OGTT (NGT/IGT/DM)	4/7/7	3/6/5	13/29/24

Data are expressed as mean ± SD

* $P < 0.05$ versus group A versus group B. ** $P < 0.01$ versus group B. *** $P < 0.001$ versus group A

NAS nonalcoholic fatty liver disease (NAFLD) activity score, *HOMA-R* homeostasis model assessment of insulin resistance, *AST* aspartate aminotransferase, *ALT* alanine aminotransferase, *HDL* high-density lipoprotein, *LDL* low-density lipoprotein, *ecd* electronegative-charge density, *SMP30* senescence marker protein-30, *OGTT* oral glucose tolerance test, *NGT* normal glucose tolerance, *IGT* impaired glucose tolerance, *DM* diabetes mellitus

(4-HNE) monoclonal antibody (1:100 dilution; Nihon Yushi, Tokyo, Japan). SMP30 and 4-HNE were detected by indirect immunoperoxidase staining using corresponding Histofine Simple Stain MAX-PO kits (Nichirei Biosciences, Tokyo, Japan) and 3, 3-diaminobenzidine (DAB) as a chromogenic substrate. After DAB staining, nuclei were counterstained with Mayer's hematoxylin. Two independent observers evaluated the intensity of immunostaining for 4-HNE as 0, 1, 2, or 3 (negative, weak, moderate, or strong, respectively).

Quantification of hepatic SMP30 content by enzyme-linked immunosorbent assay (ELISA)

A portion of each liver biopsy specimen was immediately frozen and stored at −80°C for hepatic SMP30 measurement. Frozen liver biopsy specimens were suspended in ice-cold phosphate-buffered saline (PBS; pH 7.4). After disruption by homogenization and sonication, samples were centrifuged (15,000 *g*, 15 min, 4°C) and supernatants were stored at −80°C until assay. SMP30 in supernatant fractions was determined by a sandwich ELISA using a polyclonal anti-SMP30 antibody (Cosmo Bio, Tokyo, Japan) and a monoclonal anti-SMP30 antibody. In brief, microtiter plates were coated with affinity-purified anti-SMP30 rabbit IgG (2.0 μg/ml) diluted with 10 mM carbonate buffer (pH 9.3) for 2 h at room temperature. After washing, nonspecific binding sites in each well were blocked with 10 mM carbonate buffer containing 0.5% bovine serum albumin (BSA). Standard solution (0–2,000 pg/ml recombinant SMP30) and supernatant samples diluted (1:10) with sample buffer (50 mM Tris–HCl buffer, pH 7.0, containing 200 mM NaCl, 10 mM $CaCl_2$, 0.1% Triton X-100, and 1% BSA) were added to the wells, and the plate was incubated for 2 h at room temperature. After a washing with BSA-free sample buffer, biotinylated anti-monoclonal SMP30 antibody was added to each well. The plate was incubated for 2 h at room temperature, washed, and then incubated for an additional 2 h at room temperature with streptavidin-horseradish peroxidase (HRP) diluted 1:10,000 (Vector Laboratories, Burlingame, CA, USA). After a final washing, the plate was treated for 20 min with

a substrate solution of 3,3′,5,5′-tetramethylbenzidine and H_2O_2 was added to each well and allowed to react for 15 min at room temperature. The reaction was stopped by the addition of 1 M phosphoric acid, after which optical density (OD) values at 450 nm were read with an ELISA plate reader. The detection limit of the assay was 20 pg/ml and the intra- and interassay coefficients of variation were 6.4 and 8.2% at 50 pg/ml and 4.6 and 7.0% at 500 pg/ml, respectively. The concentration of SMP30 in liver tissue was expressed based on milligrams of total protein. The protein concentration was determined using a Bio-Rad DC protein assay kit (Bio-Rad, Hercules, CA, USA) with human serum albumin as a standard.

Laboratory investigations

Blood samples were obtained in the morning after an overnight fast. Plasma glucose was measured by the glucose oxidase method and HbA1c was determined by high-performance liquid chromatography (HPLC; Arkray, Kyoto, Japan). Serum insulin (immunoreactive insulin; IRI) concentrations were measured by an immunoradiometric assay (Insulin-RIAbead II, Abbott Japan, Tokyo, Japan). The homeostasis model assessment of insulin resistance (HOMA-R) was calculated from fasting insulin and glucose levels by the following equation: HOMA-R = fasting IRI (mU/ml) × fasting plasma glucose (PG) (mg/dl)/405. Serum aspartate aminotransferase (AST), alanine aminotransferase (ALT), total cholesterol (T-Ch), high-density lipoprotein cholesterol (HDL-Ch), low-density lipoprotein cholesterol (LDL-Ch), and triglyceride (TG) were measured by enzymatic methods using a chemical autoanalyzer (Hitachi, Tokyo, Japan). Serum type IV collagen 7S was measured with a radioimmunoassay kit (Mitsubishi Chemical Group, Tokyo, Japan). Serum oxidized LDL (oxLDL) was measured with an ELISA kit (Kyowa Medex, Tokyo, Japan).

The net electronegative charge modified-LDL (emLDL) was analyzed using an agarose gel electrophoresis lipoprotein fraction system, according to the manufacturer's instructions (Chol/Trig Combo System; Helena Labs, Saitama, Japan). The percentage frequency of emLDL was calculated on a computer from the migration distance (b) of the LDL fraction in the test samples and the migration distance (a) of normal control sera, according to the following formula: emLDL density = $[b - a/a] \times 100\%$. The intraassay coefficient of variation in this method was <1%. In our preliminary study, the value of emLDL in normal healthy subjects ($n = 45$, mean age 46.5 ± SD 3.9 years) was 0.3 ± 2.6% (unpublished data). Serum lipoproteins were also analyzed by an HPLC system according to the procedure described by Okazaki et al. [21], while lipoprotein particle size was determined based on individual elution times that corresponded to peaks on the chromatographic pattern of cholesterol fractions. In this study, we defined very low-density lipoprotein (VLDL), LDL, and HDL subclasses according to lipoprotein particle size, expressed as diameter [22].

Statistical analysis

All statistical analyses were performed with Statview version 5.0 (Abacus Concepts, Berkeley, CA, USA), with data expressed as mean ± SD. When the data were not normally distributed, logarithmic transformation was performed. Differences between the groups were determined by Student's t test or one-way analysis of variance (ANOVA) with Scheffé's multiple comparison test. Categorical data were assessed by the χ^2 test. The degree of correlation between selected variables was determined by Pearson's correlation analysis or Spearman's correlation analysis. The relationship between hepatic SMP30 levels and other clinical parameters was also analyzed by stepwise multiple regression analysis using forward direction, with the F value for entry set at 4.0. A P value of <0.05 was considered statistically significant.

Results

The clinical, biochemical, and laboratory data of the three patient groups classified by NAS score are summarized in Table 1. Patients with NAS ≥ 5 had significantly lower hepatic SMP30 levels than patients with NAS ≤ 2 ($P < 0.001$) and patients with NAS of 3–4 ($P < 0.01$). Patients with NAS ≥ 5 had significantly higher HOMA-R ($P < 0.05$), serum emLDL ($P < 0.05$), and serum type IV collagen 7S ($P < 0.05$) and had lower platelet counts ($P < 0.05$) than patients with NAS ≤ 2 or patients with NAS of 3–4. There was no significant difference in the other clinical and laboratory data among the three patient groups.

Hepatic SMP30 levels were significantly and positively correlated with platelet count ($P < 0.05$), and were significantly and inversely correlated with HOMA-R ($P < 0.05$), serum emLDL ($P < 0.01$), and serum type IV collagen 7S ($P < 0.01$; Table 2). Stepwise multiple regression analysis also showed that hepatic SMP30 levels were associated with HOMA-R ($F = 4.08$) emLDL ($F = 11.19$), and type IV collagen 7S ($F = 5.23$; Table 2).

As shown in Fig. 1A, immunohistochemical staining showed strong expression of SMP30 protein in parenchymal cells in liver tissue from patients with simple steatosis (Fig. 1A-a) compared with liver tissue from patients with mild NASH (stages 0–1; Fig. 1A-b), moderate NASH (stage 2; Fig. 1A-c), and advanced NASH (stages 3–4; Fig. 1A-d). The level of hepatic SMP30 was significantly higher in patients with simple steatosis (28.5 ± 9.5 ng/mg

Table 2 Pearson's correlation and stepwise multiple regression analysis of the relationship between hepatic SMP-30 and 18 clinical variables

	Pearson's correlation	Stepwise multiple regression	
	r	β	F
Age	−0.111	–	–
Body mass index	−0.116	–	–
Systolic blood pressure	−0.034	–	–
Diastolic blood pressure	−0.040	–	–
HbA1c (%)	0.026	–	–
Fasting glucose	−0.201	–	–
Fasting insulin	−0.158	–	–
HOMA-R	−0.298*	−0.243	4.08*
AST	−0.127	–	–
ALT	−0.190	–	–
Triglyceride	−0.175	–	–
Total cholesterol	0.026	–	–
HDL cholesterol	0.031	–	–
LDL cholesterol	−0.158	–	–
Oxidized LDL (U/ml)	−0.241	–	–
Electronegative charge modified-LDL	−0.442**	−0.380	11.19**
Type IV collagen 7S	−0.350**	−0.260	5.23*
Platelet count	0.291*	–	–

* $P < 0.05$, ** $P < 0.01$

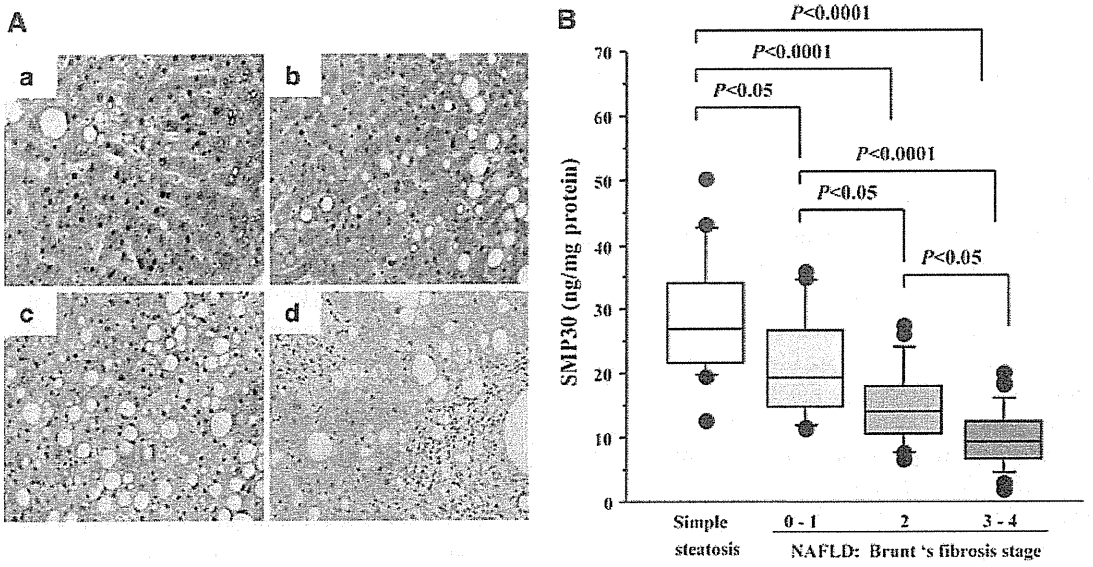

Fig. 1 **A** Immunostaining of senescence marker protein-30 (*SMP30*) in liver tissue from patients with *a* simple steatosis, *b* mild nonalcoholic steatohepatitis (NASH; stages 0–1), *c* moderate NASH (stage 2), and *d* advanced NASH (stage 3–4), ×400. **B** Hepatic SMP30 levels in patients with simple steatosis, mild NASH, moderate NASH, or advanced NASH. The *box plots* include the medians (*horizontal lines*) and interquartile ranges (*boxes*), whereas the *whiskers* represent the 10–90th percentiles, and the *dots* represent the 5–95th percentiles and 1–99th percentiles, respectively. *NAFLD* nonalcoholic fatty liver disease

protein) compared with that in patients with NASH (vs. mild; 21.2 ± 7.9, $P < 0.05$, vs. moderate; 14.9 ± 5.9, $P < 0.001$, and vs. advanced; 9.6 ± 4.6, $P < 0.001$), and was observed as decreasing in a stage-dependent manner (Fig. 1B).

The grade of fatty change evaluated with hematoxylin-eosin staining (Fig. 2a) was correlated well with the intensity of Oil Red O staining (Fig. 2b).

In this study, to estimate oxidative stress in liver tissue, we investigated the expression of 4-HNE, a marker of

lipid peroxidation products. As shown in Fig. 3a, b, the immunostaining intensity of 4-HNE in tissues from patients with NAS ≥ 5 (Fig. 3A-c and -d) was significantly greater than that seen in patients with NAS ≤ 2 (Fig. 3A-a) and patients with NAS of 3–4 (Fig. 3A-b). Spearman's correlation analysis showed that the immunostaining intensity levels of 4-HNE had a significant negative correlation with hepatic SMP30 levels ($\rho = -0.649$, $P < 0.01$; Fig. 3c).

We investigated serum lipoprotein profiles in the patients with NAS ≤ 2 ($n = 15$) and those with NAS ≥ 5 ($n = 20$). As shown in Fig. 4, levels of large VLDL and very small LDL in patients with NAS ≥ 5 were significantly higher than those in patients with NAS ≤ 2 (5.6 ± 1.3 vs. 4.5 ± 1.2 mg/dl, $P = 0.008$ and 20.4 ± 5.4 vs. 17.0 ± 4.0 mg/dl, $P = 0.047$, respectively). There was no significant difference in the other lipoprotein subclass levels between patients with mild and advanced NASH. Both large VLDL and very small LDL levels were correlated negatively with hepatic SMP30 levels ($r = -0.379$, $P = 0.024$ and $r = -0.357$, $P = 0.035$, respectively; Fig. 5).

Discussion

In the present study, we have demonstrated for the first time, by both ELISA and immunohistochemical studies, the significant reduction of hepatic SMP30 levels in a stage-dependent manner in patients with NAFLD. An additional noteworthy finding of this study is that the hepatic SMP30 level was strongly and inversely correlated with the grade of immunohistochemical staining of 4-HNE, which is an aldehydic end product of lipid peroxidation in hepatocytes. Furthermore, we also demonstrated that hepatic SMP30 levels were significantly and positively correlated with the platelet count, and were significantly and inversely correlated with HOMA-R, serum emLDL, and serum type IV collagen 7S. It is well known that increased lipotoxicity and oxidative stress in the liver play a critical role in the progression of NAFLD. Accumulated reactive oxygen species (ROS) activate nonparenchymal cells, including Kupffer cells and hepatic stellate cells [23]. By way of a paracrine mechanism, activated Kupffer cells release transforming growth factor (TGF)-β, a known profibrotic factor that has been implicated in the activation

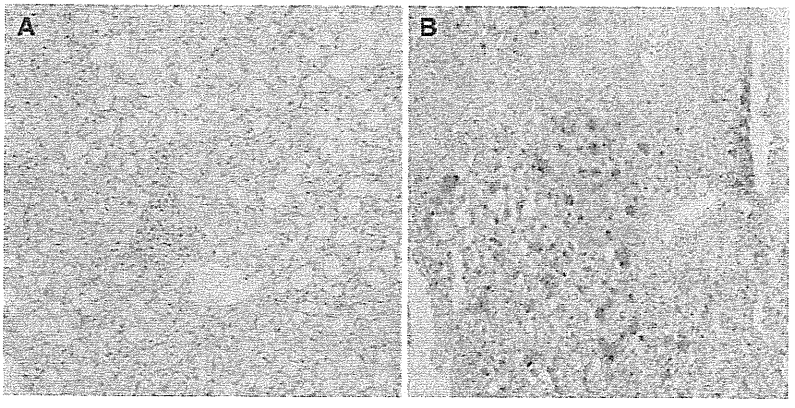

Fig. 2 **a** H&E staining in liver tissue from a patient with mild NASH. Many large fat droplets are noted around the central vein. **b** Oil Red O staining in liver tissue from a patient with large fat droplets. **a**, **b** ×200

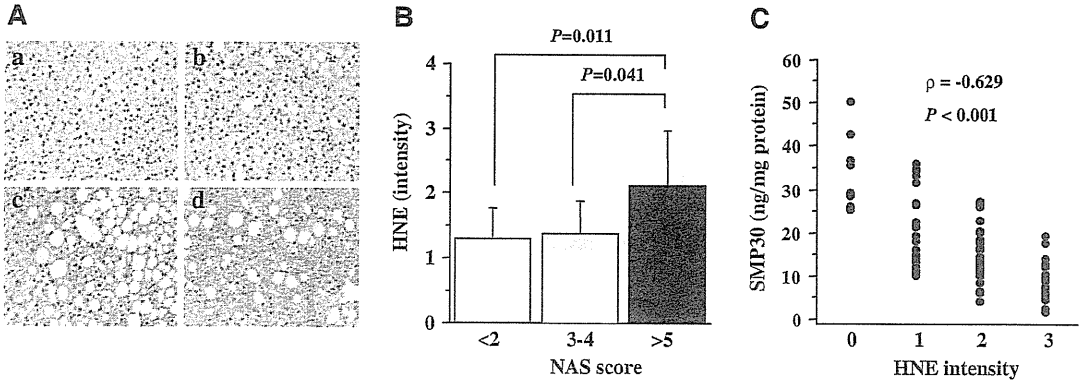

Fig. 3 **A** Immunostaining of 4-hydroxynoneral (*4-HNE*) in liver tissues from patients with *a* NAFLD activity score (*NAS*) ≤ 2, *b* NAS = 3–4, and *c*, *d* NAS ≥ 5, ×200. **B** Hepatic 4-HNE intensity in the three patient groups classified according to the NAS scores. *c* Spearman's correlation between hepatic SMP-30 and 4-HNE intensity

of other neighboring hepatic cells, including hepatic stellate cells [24]. Recently, Tomita et al. [25] reported that hepatic expression of TGF-β1 was enhanced at both early and late fibrotic stages of NASH, and that elimination of hepatic ROS accumulation in the liver decreased hepatic TGF-β1, whereas enhancement of ROS in the liver increased TGF-β1 mRNA levels. It has also been reported that 4-HNE stimulates procollagen type I synthesis in human hepatic stellate cells [26, 27]. SMP30 maintains calcium homeostasis by activating the calmodulin-dependent Ca^{2+}-pump, and has gluconolactonase activity. Several functional studies of SMP30 have demonstrated that SMP30 plays a role as an antiapoptotic protein and antioxidant [15, 17–20, 28, 29]. Therefore, our findings strongly suggest that the reduction of hepatic SMP30 is associated with the progression of hepatic fibrosis through increased oxidative stress in the liver. In our preliminary study, hepatic SMP30 was significantly decreased in hepatitis C virus (HCV)-infected patients with cirrhosis (data not shown). It is suggested that hepatic SMP30 is decreased in cirrhotic liver by other etiologies as well as NAFLD. However, it is not known whether decreased hepatic SMP30 is a result or a cause of cirrhosis. Further studies are needed to clarify this point.

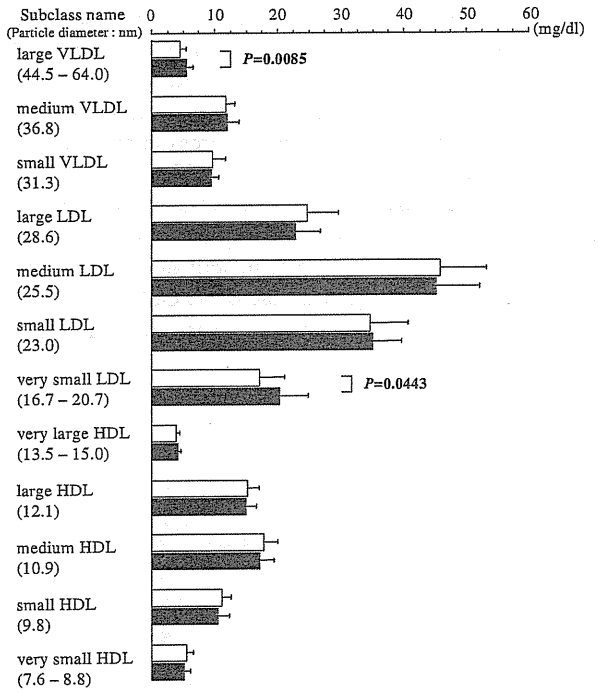

Fig. 4 Comparison of the levels of each lipoprotein subclass grouped according to particle size. The *open columns* represent data from 15 patients with NAS $\leq$ 2 and the *closed columns* represent data from 20 patients with NAS $\geq$ 5. *VLDL*, Very low-density lipoprotein; *LDL*, low-density lipoprotein; *HDL*, high-density lipoprotein

In the present study, we found that emLDL was significantly increased in an NAS-dependent fashion. Similarly, using lipoprotein profile analysis by HPLC, we also found that in patients with NAS $\geq$ 5, serum levels of both large VLDL, which corresponds to VLDL1 (Svedberg flotation, Sf 60–400), and very small LDL were significantly higher than those in patients with NAS $\leq$ 2. A noteworthy finding is that these lipoproteins were significantly and inversely correlated with hepatic SMP30. Griffin and Packard [30] and Packard [31] have demonstrated that large VLDL1 is a precursor of small dense LDL, and VLDL1 is preferentially produced in the liver during the development of insulin resistance. Adiels et al. [32, 33] have reported that hyperglycemia stimulates VLDL1 production in type 2 diabetes, and that overproduction of VLDL1 is significantly correlated with increased liver fat and plasma glucose in patients with type 2 diabetes. Previously, we reported that accumulation of cholesterol in the livers of SMP30-deficient (SMP30Y/−) mice was markedly higher than that in age-matched wild-type mice [16]. In the SMP30Y/− mice, mitochondrial damage and many fat droplets were observed in hepatocytes by electron microscopy [16]. Our present findings, taken together with these findings in the SMP30Y/− mice, lead us to speculate

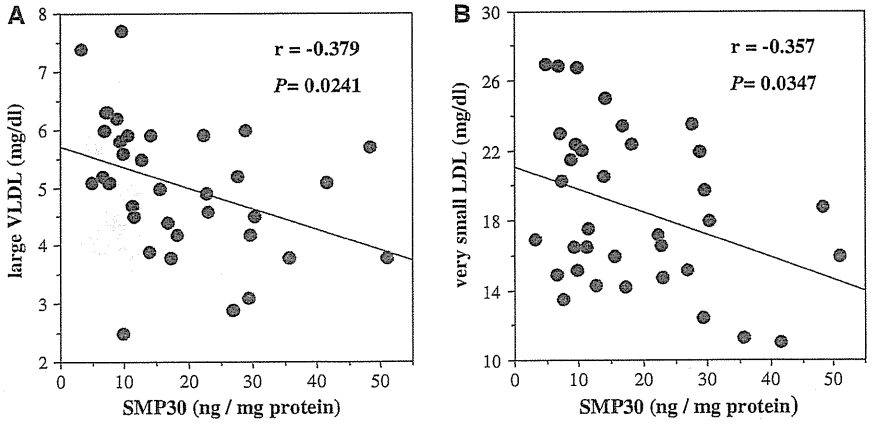

Fig. 5 Pearson's correlations between **a** hepatic SMP-30 and serum large VLDL (particle size 44.5–64.0 nm) and **b** between hepatic SMP-30 and serum very small LDL (particle size 16.7–20.7 nm)

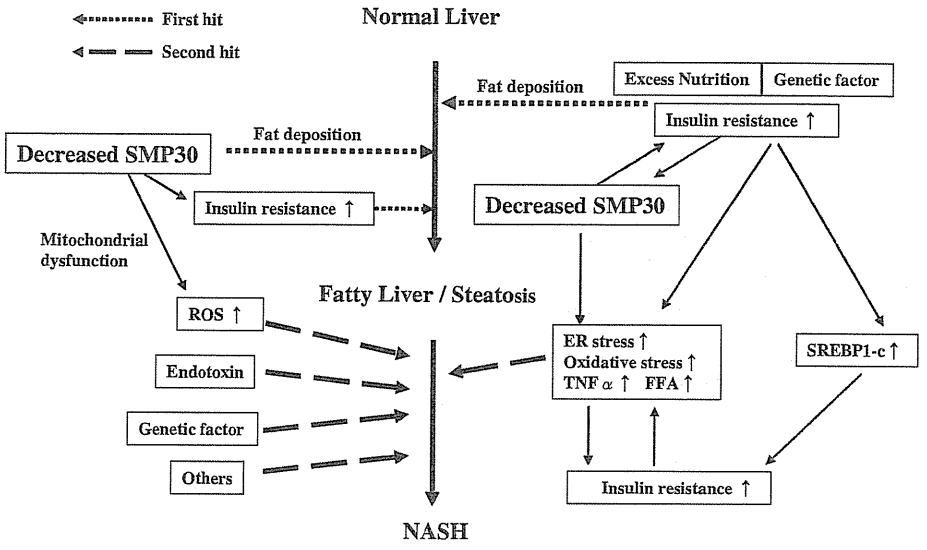

Fig. 6 Schematic diagram depicting disease progression of NAFLD according to the two-hit hypothesis, showing involvement of hepatic SMP30. *FFA*, free fatty acid; *SREBP*, sterol regulatory element-binding proteins; *TNF*, tumor necrosis factor

that steadily decreasing hepatic SMP30 levels are associated with the progression of hepatic insulin resistance.

In conclusion, the two-hit theory proposed by Day and James [9], in which the initial trigger is the hepatic accumulation of excessive fat, followed by the second hit of the development of oxidative stress, is widely advocated as a pathogenic mechanism for NASH. Therefore, our findings in the present study strongly suggest that SMP30 plays an important role in the pathogenesis of NAFLD (Fig. 6), and that increasing levels of SMP30 in the liver will serve as a promising target in the treatment of NASH.

Acknowledgments This study was supported by a Grant-in-Aid for Scientific Research (C) from the Japan Society for the Promotion of Science (Goji Hasegawa), and a Grant-in-Aid from the Ministry of Health, Labour and Welfare (Takeshi Okanoue).

References

1. Angulo P. Nonalcoholic fatty liver disease. N Engl J Med. 2002;18:1221–31.
2. Browning JD, Szczepaniak LS, Dobbins R, Nuremberg P, Horton JD, Cohen JC, et al. Prevalence of hepatic steatosis in an urban population in the United States: impact of ethnicity. Hepatology. 2004;40:1387–95.
3. Farrell GC. Non-alcoholic steatohepatitis: what is it, and why is it important in the Asia-Pacific region? J Gastroenterol Hepatol. 2003;18:124–38.
4. Ludwig J, Viggiano TR, McGill DB, Oh BJ. Nonalcoholic steatohepatitis: Mayo Clinic experiences with a hitherto unnamed disease. Mayo Clin Proc. 1980;55:434–8.
5. Kleiner DE, Brunt EM, Van Natta M, Behling C, Contos MJ, Cummings OW, et al. Design and validation of a histological scoring system for nonalcoholic fatty liver disease. Hepatology. 2005;41:1313–21.
6. Brunt EM, Janney CG, Di Bisceglie AM, Neuschwander-Tetri BA, Bacon BR. Nonalcoholic steatohepatitis: a proposal for grading and staging the histological lesions. Am J Gastroenterol. 1999;94:2467–74.
7. Chitturi S, Abeygunasekera S, Farrell GC, Holmes-Walker J, Hui JM, Fung C, et al. NASH and insulin resistance: Insulin hypersecretion and specific association with the insulin resistance syndrome. Hepatology. 2002;35:373–9.
8. Sanyal AJ, Campbell-Sargent C, Mirshahi F, Rizzo WB, Contos MJ, Sterling RK, et al. Nonalcoholic steatohepatitis: association of insulin resistance and mitochondrial abnormalities. Gastroenterology. 2001;120:1183–92.
9. Day CP, James OF. Steatohepatitis: a tale of two "hits"? Gastroenterology. 1998;114:842–5.
10. Fujita T, Uchida K, Maruyama N. Purification of senescence marker protein-30 (SMP30) and its androgen-independent decrease with age in the rat liver. Biochim Biophys Acta. 1992; 1116:122–8.
11. Ishigami A, Maruyama N. Significance of SMP30 in gerontology. Geriatr Gerontol Int. 2007;7:316–25.
12. Fujita T, Inoue H, Kitamura T, Sato N, Shimosawa T, Maruyama N. Senescence marker protein-30 (SMP30) rescues cell death by enhancing plasma membrane Ca(2+)-pumping activity in Hep G2 cells. Biochem Biophys Res Commun. 1998;250:374–80.
13. Inoue H, Fujita T, Kitamura T, Shimosawa T, Nagasawa R, Inoue R, et al. Senescence marker protein-30 (SMP30) enhances the calcium efflux from renal tubular epithelial cells. Clin Exp Nephrol. 1999;3:261–7.
14. Kondo Y, Inai Y, Sato Y, Handa S, Kubo S, Shimokado K, et al. Senescence marker protein 30 functions as gluconolactonase in L-ascorbic acid biosynthesis, and its knockout mice are prone to scurvy. Proc Natl Acad Sci USA. 2006;103:5723–8.
15. Ishigami A, Fujita T, Handa S, Shirasawa T, Koseki H, Kitamura T, et al. Senescence marker protein-30 knockout mouse liver is highly susceptible to tumor necrosis factor-alpha- and Fas-mediated apoptosis. Am J Pathol. 2002;161:1273–81.
16. Ishigami A, Kondo Y, Nanba R, Ohsawa T, Handa S, Kubo S, et al. SMP30 deficiency in mice causes an accumulation of neutral lipids and phospholipids in the liver and shortens the life span. Biochem Biophys Res Commun. 2004;315:575–80.
17. Sato T, Seyama K, Sato Y, Mori H, Souma S, Akiyoshi T, et al. Senescence marker protein-30 protects mice lungs from oxidative stress, aging, and smoking. Am J Respir Crit Care Med. 2006; 174:530–7.

18. Son TG, Zou Y, Jung KJ, Yu BP, Ishigami A, Maruyama N, et al. SMP30 deficiency causes increased oxidative stress in brain. Mech Ageing Dev. 2006;127:451–7.
19. Kondo Y, Sasaki T, Sato Y, Amano A, Aizawa S, Iwama M, et al. Vitamin C depletion increases superoxide generation in brains of SMP30/GNL knockout mice. Biochem Biophys Res Commun. 2008;377:291–6.
20. Sato Y, Kajiyama S, Amano A, Kondo Y, Sasaki T, Handa S, et al. Hydrogen-rich pure water prevents superoxide formation in brain slices of vitamin C-depleted SMP30/GNL knockout mice. Biochem Biophys Res Commun. 2008;375:346–50.
21. Okazaki M, Usui S, Ishigami M, Sakai N, Nakamura T, Matsuzawa Y, et al. Identification of unique lipoprotein subclasses for visceral obesity by component analysis of cholesterol profile in high-performance liquid chromatography. Arterioscler Thromb Vasc Biol. 2005;25:578–84.
22. Okazaki M, Usui S, Fukui A, Kubota I, Tomoike H. Component analysis of HPLC profiles of unique lipoprotein subclass cholesterols for detection of coronary artery disease. Clin Chem. 2006;52:2049–53.
23. Poli G. Pathogenesis of liver fibrosis: role of oxidative stress. Mol Aspects Med. 2000;21:49–98.
24. Matsuoka M, Tsukamoto H. Stimulation of hepatic lipocyte collagen production by Kupffer cell-derived transforming growth factor beta: implication for a pathogenetic role in alcoholic liver fibrogenesis. Hepatology. 1990;11:599–605.
25. Tomita K, Oike Y, Teratani T, Taguchi T, Noguchi M, Suzuki T, et al. Hepatic AdipoR2 signaling plays a protective role against progression of nonalcoholic steatohepatitis in mice. Hepatology. 2008;48:458–73.
26. Parola M, Pinzani M, Casini A, Albano E, Poli G, Gentilini A, et al. Stimulation of lipid peroxidation or 4-hydroxynonenal treatment increases procollagen alpha 1 (I) gene expression in human liver fat-storing cells. Biochem Biophys Res Commun. 1993;194:1044–50.
27. Parola M, Pinzani M, Casini A, Leonarduzzi G, Marra F, Caligiuri A, et al. Induction of procollagen type I gene expression and synthesis in human hepatic stellate cells by 4-hydroxy-2,3-nonenal and other 4-hydroxy-2,3-alkenals is related to their molecular structure. Biochem Biophys Res Commun. 1996;222:261–4.
28. Park JK, Jeong DH, Park HY, Son KH, Shin DH, Do SH, et al. Hepatoprotective effect of Arazyme on CCl4-induced acute hepatic injury in SMP30 knock-out mice. Toxicology. 2008;246:132–42.
29. Jeong DH, Goo MJ, Hong IH, Yang HJ, Ki MR, Do SH, et al. Inhibition of radiation-induced apoptosis via overexpression of SMP30 in Smad3-knockout mice liver. J Radiat Res (Tokyo). 2008;49:653–60.
30. Griffin BA, Packard CJ. Metabolism of VLDL and LDL subclasses. Curr Opin Lipidol. 1994;5:200–6.
31. Packard CJ. Triacylglycerol-rich lipoproteins and the generation of small, dense low-density lipoprotein. Biochem Soc Trans. 2003;31(Pt 5):1066–9.
32. Adiels M, Borén J, Caslake MJ, Stewart P, Soro A, Westerbacka J, et al. Overproduction of VLDL1 driven by hyperglycemia is a dominant feature of diabetic dyslipidemia. Arterioscler Thromb Vasc Biol. 2005;25:1697–703.
33. Adiels M, Taskinen MR, Packard C, Caslake MJ, Soro-Paavonen A, Westerbacka J, et al. Overproduction of large VLDL particles is driven by increased liver fat content in man. Diabetologia. 2006;49:755–65.

Acta Neuropathol
DOI 10.1007/s00401-009-0625-x

ORIGINAL PAPER

Involvement of peptidylarginine deiminase-mediated post-translational citrullination in pathogenesis of sporadic Creutzfeldt-Jakob disease

Byungki Jang · Jae-Kwang Jin · Yong-Chul Jeon · Han Jeong Cho · Akihito Ishigami · Kyung-Chan Choi · Richard I. Carp · Naoki Maruyama · Yong-Sun Kim · Eun-Kyoung Choi

Received: 23 July 2009 / Revised: 27 November 2009 / Accepted: 5 December 2009

Abstract Peptidylarginine deiminases (PADs)-mediated post-translational citrullination processes play key roles in protein functions and structural stability through the conversion of arginine to citrulline in the presence of excessive calcium concentrations. In brain, PAD2 is abundantly expressed and can be involved in citrullination in disease. Recently, we have reported pathological characterization of PAD2 and citrullinated proteins in scrapie-infected mice, but the implication of protein citrullination in the pathophysiology in human prion disease is not clear. In the present study, we explored the molecular and biological involvement of PAD2 and the pathogenesis of citrullinated proteins in frontal cortex of patients with sporadic Creutzfeldt-Jakob disease (sCJD). We found increased expression of PAD2 in reactive astrocytes that also contained increased levels of citrullinated proteins. In addition, PAD activity was significantly elevated in patients with sCJD compared to controls. From two-dimensional gel electrophoresis and MALDI-TOF mass analysis, we found various citrullinated candidates, including cytoskeletal and energy metabolism-associated proteins such as vimentin, glial fibrillary acidic protein, enolase, and phosphoglycerate kinase. Based on these findings, our investigations suggest that PAD2 activation and aberrant citrullinated proteins could play a role in pathogenesis and have value as a marker for the postmortem classification of neurodegenerative diseases.

Keywords Citrullination · Peptidylarginine deiminase · Creutzfeldt-Jakob disease · Prion · Astrocytes

Abbreviations

PAD	Peptidylarginine deiminase
CJD	Creutzfeldt-Jakob disease
PrP	Prion protein
CNS	Central nervous system
2-DE	Two-dimensional gel electrophoresis
MALDI-TOF mass	Matrix-assisted laser desorption/ ionization-time of flight mass
BAEE	Benzoyl-L-arginine ethyl ester
SDS	Sodium dodecyl sulfate
anti-MC	Anti-modified citrulline
GAPDH	Glyceraldehyde-3-phosphate dehydrogenase

B. Jang · J.-K. Jin · Y.-C. Jeon · H. J. Cho · Y.-S. Kim · E.-K. Choi
Ilsong Institute of Life Science, Hallym University, Anyang, Republic of Korea

B. Jang · Y.-S. Kim
Department of Microbiology, College of Medicine, Hallym University, Chuncheon, Republic of Korea

A. Ishigami
Department of Biochemistry, Faculty of Pharmaceutical Sciences, Toho University, Chiba, Japan

A. Ishigami · N. Maruyama
Tokyo Metropolitan Institute of Gerontology, Itabashi-ku, Tokyo, Japan

K.-C. Choi
Department of Pathology, College of Medicine, Hallym University, Chuncheon, Republic of Korea

R. I. Carp
New York State Institute for Basic Research in Developmental Disabilities, Staten Island, New York, USA

E.-K. Choi (✉)
Laboratory of Cellular Aging and Neurodegeneration, Ilsong Institute of Life Science, Hallym University, Anyang, Gyeonggi-do 431-060, Republic of Korea
e-mail: ekchoi@hallym.ac.kr

Published online: 16 December 2009

GFAP	Glial fibrillary acidic protein
MBP	Myelin basic protein
AD	Alzheimer's disease

Introduction

Prion diseases are a group of progressive neurodegenerative diseases that affect the central nervous system (CNS) in humans and animals. These are rare, infectious, and fatal neurodegenerative diseases that are characterized by spongiform changes, neuronal degeneration, reactive gliosis, and accumulation of disease-associated misfolded prion proteins (termed PrP^{Sc}) in the CNS [51]. In prion diseases, PrP^{Sc} is a factor in causation and is thought of as an unconventional infectious agent. Sporadic Creutzfeldt-Jakob disease (sCJD) is the most common of the human diseases, accounting for approximately 85% of human prion cases; it occurs at a rate of approximately one per million [34]. The etiological factor of sCJD remains unknown; in contrast, variant CJD is transmitted from bovine spongiform encephalopathy, and familial CJD (fCJD) is caused by a point mutation at a codon of the prion protein [1, 51].

The post-translational modifications of various proteins are important events required in the regulation of many cellular processes. Aberrant and excessive modifications can provoke abnormal conditions; in particular, these modifications have emerged as key events of CJD development and pathogenesis. These modifications include glycosylation, nitration, phosphorylation, and lipoxidation [17, 20, 45, 46]. Among various post-translational modifications, citrullination (or deimination) is an irreversible process that converts protein-bound arginine residues to citrulline which results in loss of their positive charge, provokes a conformational change, and alters the isoelectric point (*p*I) value and electrophoretic-mobility [58]. Peptidylarginine deiminases (PADs) regulate this process by their activation along with up-regulation of intracellular calcium (Ca^{2+}) distribution [60]. PADs are found as five different isoforms (types 1–4, and 6) that are distinct in substrate and tissue specificity [60]. Among them PAD2 and PAD4 are localized in the CNS [24, 25, 36, 40, 60, 62] and PAD2 is also ubiquitously distributed in other mammalian tissues such as muscle, dermis, spleen, and hematopoietic cells [37, 60]. Especially PAD2 is abundantly expressed in brain which citrullinates various cytoplasmic proteins such as glial fibrillary acidic protein (GFAP) and myelin basic protein (MBP) [24, 38]. PAD2 has been reported to contribute to pathogenic events in abnormal conditions [5, 7, 24, 25, 32, 38], and is abundantly increased in reactive astrocytes during several neurodegenerative conditions [24, 25, 43]. Distinctively, PAD4 is the only type of PAD that has a nuclear localization signal sequence at N-terminal domain [2], resulting in localization in cell nuclei where the enzyme citrullinates histones [36, 41, 61]. Since the five Ca^{2+}-binding sites were found in PAD4 by structural analysis [2] and were conserved with several other isoforms [37], it is presumed that PAD2 also contains five Ca^{2+}-binding sites. Under abnormal conditions, PADs-mediated citrullinations have been shown to affect various biological functions, such as the change of proteolytic susceptibility, binding affinity to target molecules, inflammatory processes induced by autoantibodies, regulation of gene expression, and cellular structural changes [31, 35, 49, 50, 61].

Increased citrullination and/or upregulated PAD have been reported in a number of human diseases including multiple sclerosis [36, 38, 43], rheumatoid arthritis [23, 32], Alzheimer's disease (AD) [24], cancer [10, 11], dermatosis [37, 60], and an experimental mouse model of prion disease [25]. The occurrence of citrullinated proteins is associated with disease development or progression, and it could serve as a useful marker or therapeutic target for human diseases.

Recently, we reported pathological characterization of PAD2 and citrullinated proteins that were abnormally accumulated in various brain regions of ME7 scrapie-infected mice [25]. For human prion diseases, the role of citrullination remains to be assessed. In the present study, we explored the molecular and biological involvement of PAD2 and citrullinated proteins in frontal cortex of patients with sCJD.

Materials and methods

Patients

Human brain tissues were obtained from the Biosafety Level-III Autopsy Center for CJD (Hallym University Sacred Heart Hospital, Republic of Korea). The sliced brain tissues were stored at −80°C until analysis. The study was approved by the Institutional Review Board at Hallym University. The pathologic features of the CJD patients are summarized in Table 1 and Fig. 1.

Western blot analysis

Brain tissues were homogenized in 50 mM Tris–HCl, pH 7.4, 150 mM NaCl, 1 mM EDTA, 1 mM sodium vanadate, 1% Triton X-100, 1% Nonidet P-40, 0.25% sodium deoxycholic acid, and protease inhibitors (Roche diagnostics, Indianapolis, IN, USA). For detection of PrP^{Sc}, samples were digested with 20 μg/ml proteinase-K (PK)

Table 1 Clinical details of controls and CJD patients specimens

No.	Diagnosis	Sex	Age	Brain weight (g)	Postmortem interval (h)
1	Non-CJD	M	83	1,220	12.0
2	Non-CJD	F	67	1,400	4.0
3	Non-CJD	M	71	1,225	7.0
4	Non-CJD	M	55	1,280	12.0
CJD1	Sporadic	M	77	1,600	2.5
CJD2	Sporadic	M	49	1,150	120.0
CJD3	Sporadic	F	66	1,380	13.0
CJD4	Familial	F	66	1,450	13.5

All non-CJD cases are normal brains. Familial CJD has a point mutation of valine to isoleucine at codon 203 of the prion protein

for 40 min at 37°C and then were probed with mouse monoclonal anti-PrP (3F4, 1:500) [29]. For detection of citrullinated proteins, 50 μg of protein was subjected to 12% SDS–PAGE, transferred to PVDF membrane followed by incubation in modification reagent [1 v of a mixture of 1% diacetyl monoxime/0.5% antipyrine/1 M acetic acid, and 2 v of a mixture of 85% H_3PO_4/98% H_2SO_4/H_2O (20/25/55) containing 0.1% $FeCl_3 \cdot 6H_2O$] and probed with a rabbit polyclonal anti-modified citrulline antibody (anti-MC) at 1:1,000 (Upstate, Lake Placid, NY, USA) as described previously [54]. For the detection of other target proteins, the transferred PVDF membranes were directly probed with mouse monoclonal anti-PAD2 (1:5,000) [56], rabbit polyclonal anti-GFAP (1:7,000, Dr. Ishigami generation) or rabbit polyclonal anti-GAPDH (1:1,000) (Santa Cruz Biotechnology, Santa Cruz, CA, USA). The membranes were then incubated with the appropriate secondary antibody-conjugated HRP. Bound antibodies were visualized by chemiluminescent substrate as described by the manufacturer (Amersham Biosciences, Piscataway, NJ, USA).

Immunohistochemistry

Neutral buffered formalin-fixed brains were cut into 6-μm thick slices and the sections were used for immunohistochemical staining. For staining of citrullinated proteins, the experiment was performed as described previously [25]. For negative control of staining of citrullinated proteins, the sections were incubated with dH_2O instead of 1 v of a mixture of 1% diacetyl monoxamine, 0.5% antipyrine, and 1 N acetic acid. After incubation with primary antibodies including mouse monoclonal anti-PrP (3F4, 1:200), rabbit polyclonal anti-GFAP (1:500, Dako, Copenhagen, Denmark), mouse monoclonal anti-PAD2 (2110, 1:100), and rabbit polyclonal anti-MC (1:400), the sections were washed and then treated sequentially with biotinylated anti-mouse IgG or anti-rabbit IgG, and then incubated with avidin–biotin peroxidase complex using the ABC kit (Vector, Burlingame, CA, USA), developed with 0.003% 3,3-diaminobenzidine and 0.03% H_2O_2 in 50 mM Tris buffer, and finally hematoxylin-counterstained sections were examined under light microscope (BX51; Olympus, UK). For immunofluorescence staining, primary antibodies-exposed sections were labeled with LRSC-conjugated donkey anti-rabbit IgG (1:200) or FITC-conjugated goat anti-mouse IgG (1:200) (Jackson ImmunoResearch, West Grove, PA, USA),

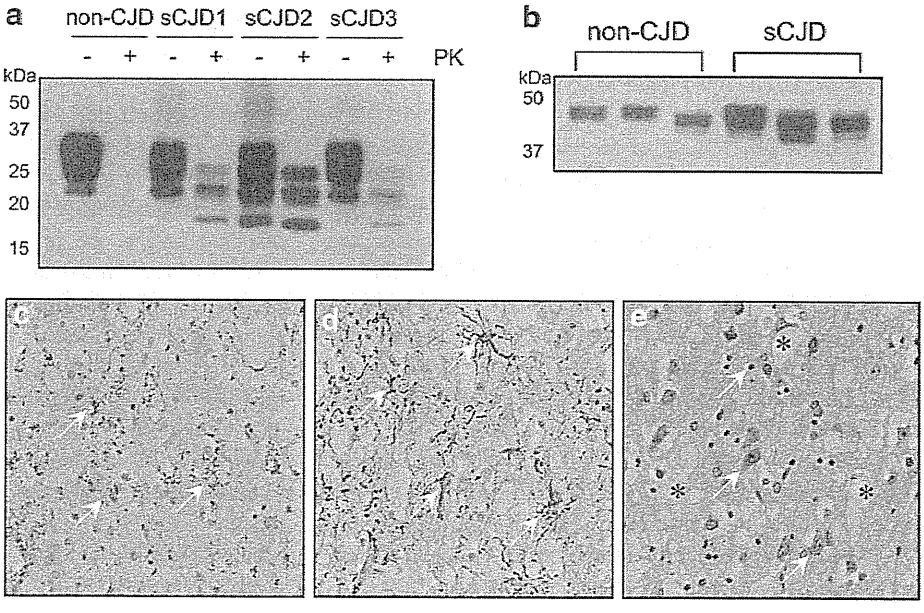

Fig. 1 Pathological characterization of brain samples from sCJD patients. **a** Proteinase K-(PK)-resistant PrP^{Sc} analysis by Western blotting using anti-PrP antibody. **b** Western blot analysis of GFAP expression using anti-GFAP antibody. **c–e** Histological characterizations including PrP^{Sc} deposition in the PK-treated brain slice (**c**), cell bodies and processes of reactive astrocytes (**d**), and vacuolation by hematoxylin–eosin staining (**e**) in frontal cortex of sCJD patients. *Arrows* indicate PrP^{Sc} (**c**), GFAP-positive astrocytes (**d**), and cell body and nucleus of neuronal cell or glial cell in the section. *Asterisks* indicate vacuoles as distinct holes. Original magnification ×20

and then observed with confocal laser scanning microscopy (LSM510; Carl Zeiss, Oberkochen, Germany).

Measurement of PAD activity

In order to determine PAD activity, 400 μg of brain proteins from non-CJD and CJD patients were incubated with the reaction mixture containing 100 mM Tris–HCl, pH 7.5, 10 mM $CaCl_2$, 5 mM dithiothreitol (DTT) with or without 10 mM benzoyl-L-arginine ethyl ester (BAEE) (Sigma–Aldrich, St. Louis, MO, USA) at 50°C for 1 h. The reaction was then stopped by adding final 1 mol/L perchloric acid. Samples were cooled down on ice for 20 min and then centrifuged at 18,000×*g* for 5 min at room temperature. 80% (v/v) supernatants were mixed with color developing reagents [1 v of a mixture of 80 mM diacetyl monoxime and 2 mM thiosemicarbazide (Sigma) in dH_2O, and 3 v of a mixture of 85% H_3PO_4/98% H_2SO_4/H_2O (33/20/47) containing 0.1% $FeCl_3 \cdot 6H_2O$] and incubated at 95°C for 15 min. To determine the value of PAD activity, samples were cooled to room temperature and then the absorbance was monitored at 534 nm by ELISA reader (VersaMax, Molecular Devices, Sunnyvale, CA, USA). One unit of the enzyme is defined as the amount of enzyme that deiminates 1 μM of BAEE (Sigma, St. Louis, MO, USA) by 1 mg of brain homogenates in 1 min at 50°C. For detection of deiminated bovine serum albumin (BSA) by brain-derived PAD, 10 μg of each brain homogenate was incubated with 500 μg of BSA as a substrate in 100 mM Tris–HCl, pH 7.6 buffer containing 10 mM Ca^{2+} and 5 mM DTT at 37°C for 30 min to 2 h. Deiminated BSA (40 μg) was detected by Western blotting using an anti-MC antibody.

Two-dimensional electrophoresis (2-DE) and matrix-assisted laser desorption/ionization-time of flight (MALDI-TOF) mass analysis

To perform 2-DE, 150 μg of protein was rehydrated with 7 cm immobilized pH gradient (IPG) strips (pH 3–10 or pH 4–7) in rehydration sample buffer (Bio-Rad, Hercules, CA, USA) for 12 h at 20°C. Isoelectric focusing was conducted at 50 V for 4 h rapidly, 250 V for 20 min rapidly, 2,000 V for 40 min linearly, and increased to a maximum of 4,000 V for 2 h linearly, and then run to accumulate a total of 18,000 Vhours rapidly using 2-D system (PROTEAN IEF CELL; Bio-Rad). Focused IPG strip was equilibrated and was then processed for 2-DE in 12% SDS–PAGE as per manufacturer's protocols. The 2-DE gels were stained by Coomassie brilliant blue G-250 (Bio-Rad) or by Western blot using anti-citrullinated antibody. To identify the citrullinated proteins, the immunoblotting-matched protein spots were excised, and then trypsin digested and MALDI-TOF mass spectrometry analysis was performed as previously described [25].

Data presentation and statistical analysis

Statistical graphs and data were displayed as mean ± standard error of the mean. The probability of statistical differences between non-CJD and sCJD groups was determined by a two-sample *t* test (two-sided) for means. Statistical differences were considered significant at $*P < 0.05$, $**P < 0.01$, and $***P < 0.001$.

Results

Clinical features of CJD patients

To evaluate aberrant citrullination and PAD2 in CJD brains, we have tested PrP^{Sc} accumulation, astrogliosis and spongiform degeneration using brain tissues from normal conditions (non-CJD) and patients with sCJD, and fCJD (Fig. 1 and Table 1). The fCJD case possesses a point mutation of valine to isoleucine at codon 203 of the prion protein as demonstrated previously [48]. PK-resistant PrP^{Sc} was detected in all cases of sCJD (Fig. 1a), and PrP^{Sc} was widely accumulated in PK-treated brain slice of the frontal cortex of sCJD (Fig. 1c). We also confirmed the increased expression of GFAP (Fig. 1b, d), which showed a reactive state of astrocytes in sCJD brains. Next, spongiform degeneration in the sections of sCJD brain was observed by hematoxylin–eosin staining (Fig. 1e). Similar observations of neuropathological features have been found in other cases, including fCJD that were used in this study (data not shown).

Upregulation of PAD2 in reactive astrocytes in patients with sCJD

In an experimental mouse model of prion disease, the expression level of PAD2 was especially high at the end stage of scrapie incubation period and was correlated with disease progression [25]. To extend this finding to human diseased brains, we investigated the expression level of PAD2 by Western blot analysis using tissue from the frontal cortex. As shown in Fig. 2a, b, the expression of PAD2 was significantly increased in the brains of sCJD patients compared to non-CJD cases. Next, to investigate the cellular localization of PAD2, we carried out immunohistochemical and immunofluorescent staining. Increased immunoreactivity of PAD2 was detected in the brains of sCJD compared to non-CJD cases (Fig. 2c) and was predominantly found in reactive astrocytes (Fig. 2d). These results confirmed our previous finding that PAD2 was significantly increased in brain and mainly localized in reactive astrocytes of scrapie-

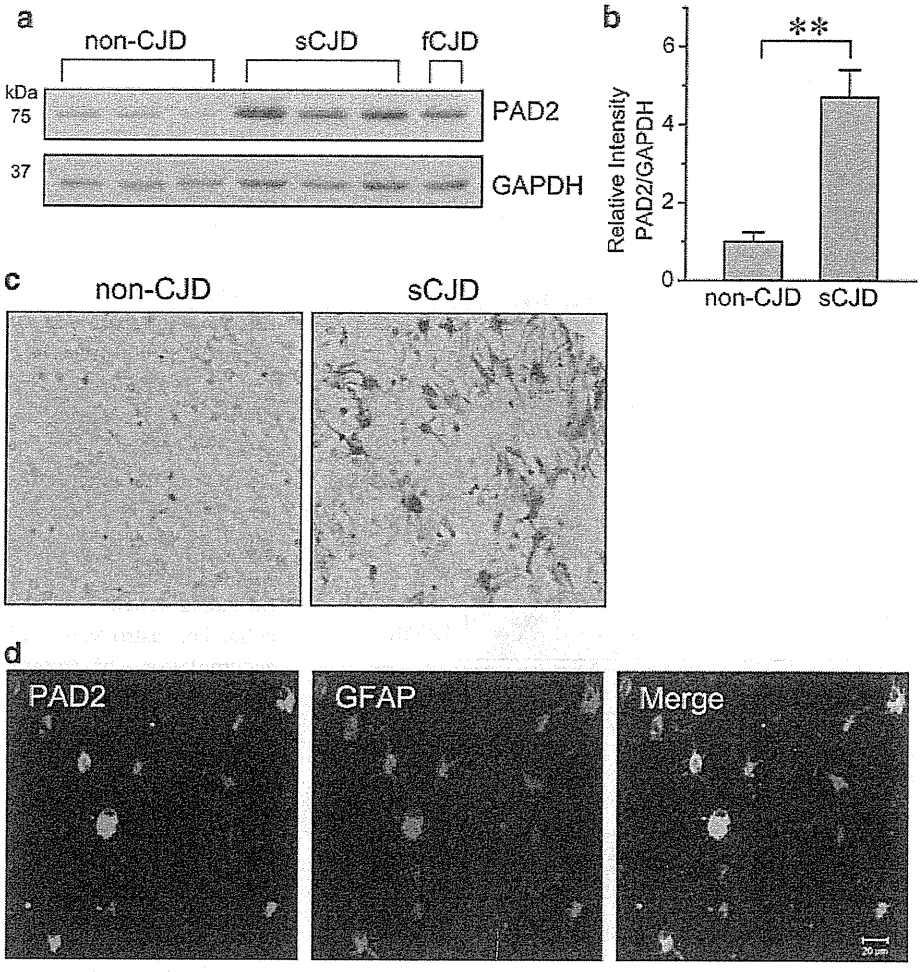

Fig. 2 Expression level of PAD2 and its cellular localization. **a** PAD2 protein was detected in frontal cortex of non-CJD and sCJD groups by Western blot analysis. GAPDH was used as a loading control. **b** PAD2 expression was normalized with GAPDH by Image J software (http://rsb.info.nih.gov/ij/). $^{**}P < 0.01$. **c** Immunohistochemical staining of PAD2 in frontal cortex of sCJD and non-CJD. Original magnification ×20. **d** Co-localization of PAD2 (*green*) and GFAP (*red*) in frontal cortex of sCJD. *Scale bars* 20 μm

infected mice [25]. Recently, it has been reported that both PAD2 and PAD4 are expressed in brains of multiple sclerosis patients [36, 62]. PAD4 was found in nuclei and at increased levels in myelin where there was an increase in citrullination of proteins. To confirm whether PAD4 is expressed and the expression level is changed in frontal cortex of patients with sCJD, we carried out subcellular fractionation to obtain cytosolic and nuclear fractions and then analyzed the expression level of PAD4 by Western blot analysis with two different PAD4 antibodies, which are specific for center or C-terminal region of PAD4. In this study, PAD4 was neither detected in whole brain homogenates nor in the nuclear fractions of brains of non-CJD or sCJD (data not shown). This result suggests that PAD2 is the main form of PADs expressed in frontal cortex of patients with sCJD.

Elevated PAD enzyme activity in frontal cortex of patients with sCJD

To establish if enzymatic activity is correlated with the increase in PAD2 expression, the enzyme activity of PAD was analyzed using brain homogenates from non-CJD and sCJD by in vitro citrullination assay with arginine analog, BAEE. As shown in Fig. 3a, PAD activity was significantly elevated by approximately 3.1-fold in sCJD brains (4.50 ± 1.09 units) compared with non-CJD brains (1.45 ± 0.13 units). In the case of fCJD, PAD activity was also slightly increased (2.52 unit) compared to non-CJD brains (data not shown). Next, to test and confirm the increased PAD activity in sCJD brains, we examined in vitro citrullination of BSA, a natural protein, using each brain homogenates under efficient Ca^{2+} concentration. To diminish intrinsic citrullinated proteins in human brain, the reaction was performed on the basis of the ratio of the protein amount in 1 μg of brain homogenates to 50 μg of BSA. The results show that the level of citrullinated BSA increased in a time-dependent manner when BSA was incubated with the homogenates of sCJD brains (Fig. 3b, c). In contrast, the level of citrullinated BSA exposed to non-CJD brain homogenate remained low throughout the incubation (Fig. 3b, c). Taken together, these results showed that both expression of PAD2

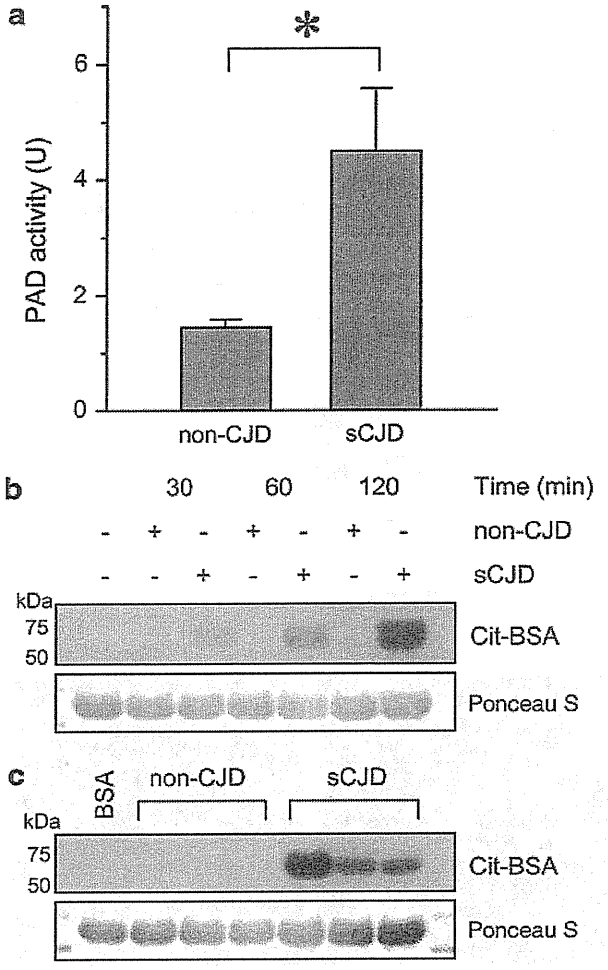

Fig. 3 Enzymatic activity of brain-derived PAD. **a** Comparison of PAD activity using BAEE as an arginine derivative in non-CJD and sCJD groups ($n = 3$/each group, $^*P < 0.05$); **b**, **c** Brain PAD-mediated deimination of BSA, which was used as a natural protein substrate. Time-dependent increase of BSA deimination (**b**) and its extensive deimination at 2 h (**c**) by incubation with sCJD brain homogenates. *Lane 1* BSA, *Lanes 2–7* BSA incubated with brains of non-CJD or sCJD. Deiminated BSA was confirmed by Western blotting with anti-MC antibody. Ponceau S staining shows equal loading volume

protein and its enzyme activity were increased in sCJD brains.

Accumulation of citrullinated proteins and their cellular localization in the brains of sCJD patients

Based on the above results, we examined whether upregulated PAD2 in sCJD brains can be correlated with the generation of citrullinated proteins. As shown in Figs. 4a, b, accumulations of citrullinated proteins occurred more extensively in patients with sCJD compared to non-CJD. This finding is consistent with our previous result showing that the citrullinated proteins were abnormally accumulated at the end stage in brains of scrapie-infected mice [25]. In the next experiments, we performed immunohistochemical staining using serial sections of each brain to confirm the cellular localization of citrullinated proteins. The immunoreactive intensity of citrullinated proteins was higher in brains of sCJD patients than in brains of non-CJD patients; the staining was mainly localized in GFAP-positive astrocytes (Fig. 4c). Brain slices were not stained by anti-MC antibody when formalin-fixed sections were treated with dH_2O rather than a mixture of diacetyl monoxamine and antipyrine in acetic acid prior to exposure to antibody (Fig. 4d). This experiment demonstrates that citrullinated proteins were aberrantly accumulated in reactive astrocytes of sCJD brains.

To confirm whether the citrullinated proteins and PAD2 are co-localized in reactive astrocytes, we performed immunostaining using serial sections of sCJD brain. As shown in Fig. 5, immunoreactive signals for PAD2, citrullinated proteins, and GFAP were found colocalized in cells, i.e., astrocytes. This observation demonstrates that accumulation of citrullinated proteins by increased expression of PAD2 is a major event in reactive astrocytes in brains of patients with sCJD.

Identification of citrullinated proteins in brains of sCJD patients

To identify citrullinated proteins in brains of sCJD patients, we carried out 2-DE on pH 3–10 IPG strips using brain homogenates from non-CJD and sCJD followed by Coomassie staining (Figs. 6a, b, d, e) and Western blotting with an anti-MC antibody for detection of citrullinated proteins (Fig. 6c, f). As seen in Fig. 6c, citrullinated proteins were broadly distributed by *p*I value and molecular weights and were clustered in neutral and basic pH ranges. To optimize the resolution of the neutral pH spots, we performed isoelectric focusing using pH 4–7 IPG strips. In the pH 4–7 range (Fig. 6d–f), separation of citrullinated proteins increased, and they were more easily distinguished than in the pH 3–10 range. Using an antibody to modified citrulline, we detected at least 30 citrullinated spots in the brain of a sCJD patient that were not seen in non-CJD brains. By peptide mass fingerprint analysis using MALDI-TOF mass spectrometry, the citrullinated spots were identified as proteins that are listed in Table 2. Although we could not identify all citrullinated spots because of their low concentration and/or inability to match in a subsequent database search, we could identify various citrullinated candidates including vimentin, GFAP, enolase 1, aldolase A, MBP, cyclophilin A, and phosphoglycerate kinase. These candidates are also known to be citrullinated in various abnormal conditions such as AD, rheumatoid arthritis, glaucoma,

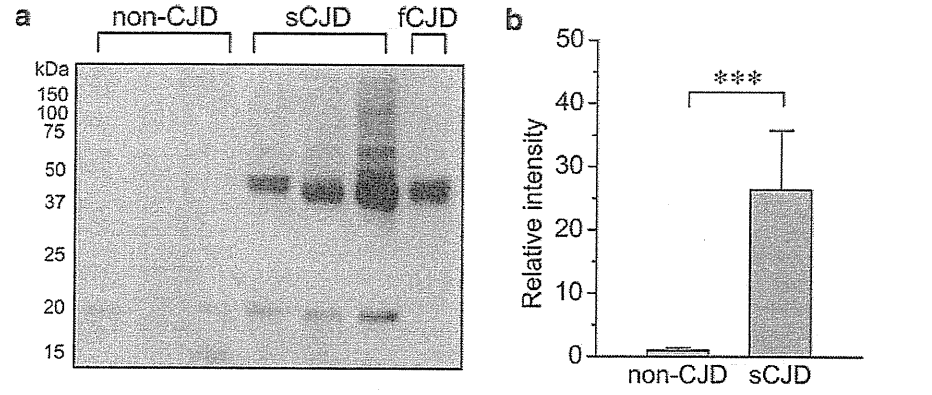

Fig. 4 Accumulation of citrullinated proteins and their cellular localization. **a** Detection of citrullinated proteins using chemically modified membrane labeled with anti-MC antibody. **b** Relative density in non-CJD and sCJD brain samples after normalization with GAPDH. Immunohistochemical staining of citrullinated proteins of non-CJD and sCJD brain samples (**c**) and negative control: section from a sCJD brain incubated with dH_2O rather than diacetyl monoxamine and antipyrine in acetic acid prior to staining with anti-MC antibody (**d**). Original magnification ×20

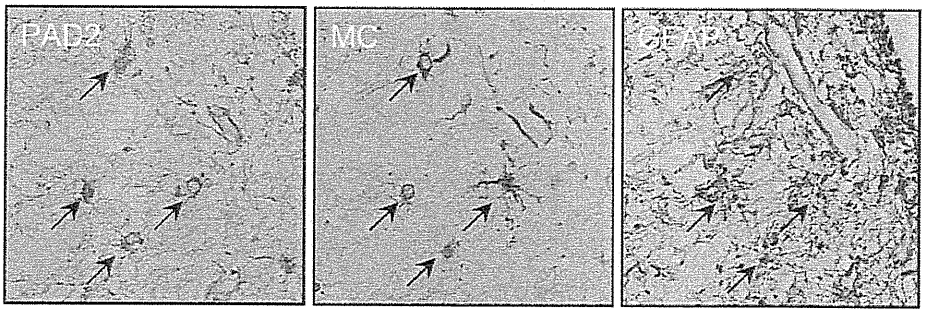

Fig. 5 Immunostaining of PAD2, citrullinated proteins, and GFAP using brain serial sections of sCJD patient. *Arrows* indicate co-localization of PAD2, citrullinated proteins (MC), and reactive astrocytes (GFAP). Original magnification ×20

scrapie infection, and multiple sclerosis [7, 24, 25, 32, 63]. Interestingly, spots including 2 and from 12 to 17, which were identified as GFAP, showed different migration pattern compared to theoretical value. Proteolytic cleavage of GFAP has been documented in various models of neurodegeneration [19, 39], which show marked astrocytic gliosis yielding GFAP fragments of molecular masses ranging from ~20 to 48 kDa. These results can explain this difference of migration pattern between theoretical information and the properties of proteins in nature.

Discussion

Although altered biochemical properties of several proteins following citrullination have been described [31, 35, 49, 50, 61], it is not clear how PAD-dependent citrullination leads to pathophysiological changes in cells. A number of researchers have evaluated the possible role of citrullination in the pathogenesis and diagnosis of diseases [23–25, 32, 37, 38]. Our recent study has revealed that prion infection induced the abnormal accumulation of citrullinated proteins by activated Ca^{2+}-dependent PAD2 in an experimental mouse model of prion disease [25], and it has led us to examine postmortem brains of a human prion disease, CJD. In the current study, we demonstrated that in brains of sCJD patients, citrullinated proteins increased, and this was associated with higher levels of PAD2 expression and increased enzymatic activity. It has been shown that prion infection induced Ca^{2+} dyshomeostasis and Ca^{2+}-mediated neurophysiological dysfunction by altering Ca^{2+} signaling molecules such as CaMK II and Ca^{2+} channels [27, 28, 53, 57]. It is clear that the activation of the deiminating activity of PAD requires Ca^{2+} as shown

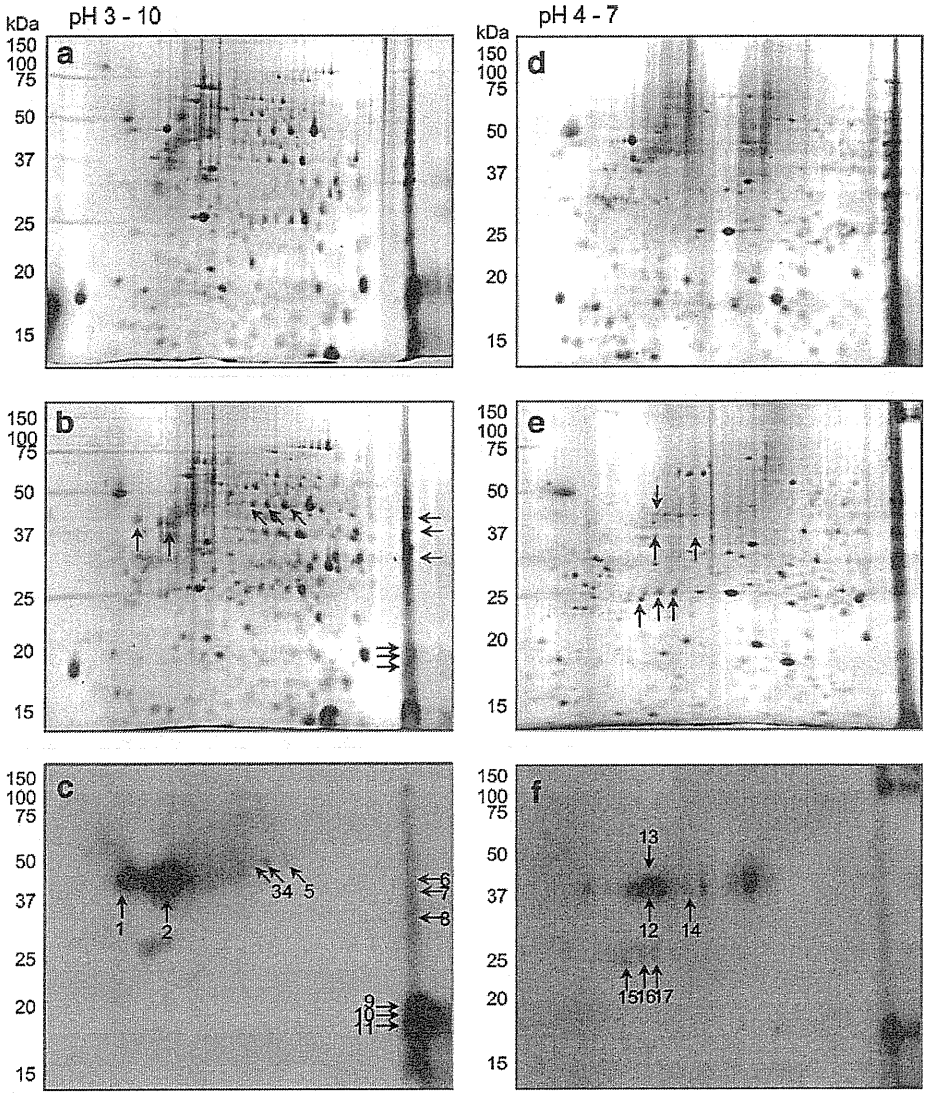

Fig. 6 2-DE analysis of brain proteins from non-CJD and sCJD. Proteins were separated on pH 3–10 (**a–c**) and pH 4–7 (**d–f**) IPG strips. **a**, **b**, **d**, **e** Coomassie staining of 2-DE gels. **c**, **f** Anti-MC antibody-labeled brain samples from patients with sCJD. **a**, **d** Control. **b**, **c**, **e**, **f** sJCD. *Arrows* indicate matched citrullinated spots and protein spots, and serial numbers were used to distinguish subsequently identified citrullinated proteins

by the fact that in vitro PAD activation is blocked by EDTA. In addition, Ca^{2+} seems to play a role in the regulation of PAD transcriptional levels [6]. Taken together, these findings along with our results indicate that Ca^{2+} imbalance in human prion diseases including sCJD may control PAD2 expression and its activity leading to citrullination of various proteins.

PAD2 is expressed at a high level in brain and has been found in glial cells [24, 25, 60]. In normal status, astrocytes play a decisive role as the linker between neurons and blood vessels [65] and act to supply the oxygen and energy sources via internal stores and vasodilatation to support neuronal activity [8, 65]. These mechanisms are involved in increases of intracellular Ca^{2+} in astrocytes, and these events trigger Ca^{2+} waves to neighboring astrocytes [12, 16, 65]. Ca^{2+} signaling in astrocytes may lead to activation of PAD2 and citrullination of its intracellular targets.

Glial cell activation is a prominent response to brain injury; astrocytes show altered shapes, enlargement of cell bodies and thickened cell processes [47]. These pathologic changes are characteristic of the astrocytosis seen in prion diseases. In our previous [25] and current immunohistochemical analyses, we demonstrated that PAD2 and citrullinated proteins were predominantly localized in reactive astrocytes. Reactive astrocytosis is accompanied by activation and upregulation of various proteins with potent biological effects: L-type Ca^{2+} channels, various ionotropic/metabotropic receptors, PAD2, and its well-known substrates including GFAP and vimentin [3, 14, 18, 21, 25]. In both human and mouse models of prion disease, increased PAD2 expression and high levels of accumulated citrullinated proteins are principally found in reactive astrocytes. The reactive status reflects abnormal brain changes, such as those in prion diseases. The current

Table 2 Summary of identified citrullinated proteins in frontal cortex of sCJD

Spot no.	Identification	Sequence coverage (%)	*p*I	kDa	NCBI accession no.	*Z* value
1	Vimentin	20	4.8	41.66	AAA61281.2	1.55
2	Glial fibrillary acidic protein	21	5.5	49.79	AAH62609.1	1.15
3	Enolase 1	15	7.0	47.49	NP_001419.1	1.57
4	Enolase 1	33	7.0	47.49	NP_001419.1	2.36
5	Enolase 1	32	7.0	47.49	NP_001419.1	2.35
6	Phosphoglycerate kinase 1	22	8.6	44.98	CAG32997.1	1.05
7	Aldolase A	22	8.7	39.71	CAA30979.1	1.34
8	Carbonyl reductase 1	24	8.9	30.64	NP_001748.1	1.37
9	Neuropolypeptide h3	57	9.0	16.06	AAD14234.1	1.86
10	17.3K Myelin basic protein	19	11.1	17.33	AAA59559.1	1.37
11	Cyclophilin A	33	8.1	18.21	CAG32988.1	1.65
12	Glial fibrillary acidic protein	22	5.4	49.79	AAH62609.1	1.73
13	Glial fibrillary acidic protein	24	5.4	49.79	AAH62609.1	1.20
14	Glial fibrillary acidic protein	19	5.4	49.79	AAH62609.1	1.48
15	Glial fibrillary acidic protein	24	5.4	49.79	AAH62609.1	1.15
16	Glial fibrillary acidic protein	23	5.4	49.79	AAH62609.1	1.26
17	Glial fibrillary acidic protein	28	5.4	49.79	AAH62609.1	2.32

Z value and its corresponding confidence are following: 1.037, 85%; 1.282, 90.0%; 1.645, 95.0%; 2.326, 99.0%; 3.090, 99.9%. *p*I, isoelectic point. The values of *p*I and molecular weight (kDa) follow theoretical value

findings support the concept that increased expression of PAD2 and the associated aberrant citrullination are involved in the induction of pathologic changes seen in patients with sCJD.

In the normal brain, there is citrullination of GFAP and MBP [42, 63], however, in various acute and progressive neurodegenerative diseases, hypercitrullination of various proteins including GFAP and MBP is seen [5, 24, 25, 38]. In our and other studies, brain-expressed PAD readily deiminates several structural and glycolytic proteins such as vimentin, GFAP, MBP, and enolase [24, 25, 38]. In CJD patients, glial cells including astrocytes and oligodendrocytes are the primary responders to neurological stress. Disturbed Ca^{2+} homeostasis in these cell types can lead to PAD activation which, in turn, can exacerbate abnormal accumulation of citrullinated proteins. Nevertheless, it is unknown whether these citrullinated proteins play a key role in pathophysiological status of reactive astrocytes and oligodendrocytes or are merely concomitant effects of activation of PAD. In addition, although citrullinated forms of astrocyte-specific GFAP have been reported in various neurodegenerative conditions [24, 25, 43], a functional role for citrullinated GFAP in CNS has not been elaborated. In Figs. 1- and 2-DE results, the GFAP protein actually runs on gels at ~25 and 37–50 kDa compared to molecular weight value of 50. GFAP has been known to yield bands at lower molecular weights [44], which are thought to be proteolytic fragments induced by Ca^{2+}-mediated protease [13, 19] and caspase 3 [39]. Thus, further characterization of the effect of citrullinated GFAP on its proteolytic processing should be addressed.

PAD2 has been considered the main type of PADs in brain, but PAD4, the isotype highly expressed in white blood cells [41, 59, 60], was recently found in fractions of nuclear and myelin from brains of multiple sclerosis patients and demyelinating animal models [36, 40, 62]. PAD4 contains a classical monopartite nuclear localization signal sequence at N-terminal [2] and is thus involved in citrullination of nuclear proteins such as histone H2A, H3, and H4 [36, 41, 61]. In addition, it has been reported that the increased PAD2 and PAD4 are important factors in increased citrullinated proteins as well as in the pathogenesis of MS [62]. However, in our expanded study, we could not detect either PAD4 or citrullinated histone H3 in frontal cortex of control or CJD brains using two different PAD4-specific antibodies (data not shown). Therefore, it is likely that the major citrullination-inducing PAD isotype in the brain of CJD in our study is PAD2, as shown by the finding that PAD2 knock-out mice did not show citrullination in brain [52], and brain-derived PAD primarily targets arginine residues of cytoplasmic proteins for citrullination [5, 25]. However, the involvement of PAD4 cannot be excluded.

Although abnormal accumulation of citrullinated proteins has been reported in various neurodegenerative conditions including prion diseases, AD, multiple sclerosis,

and kainic acid administration [4, 5, 24, 25, 36], it remains unknown whether the accumulation level of citrullination is different and whether specific citrullinated proteins are present in these neurodegenerative conditions. In our expanded study for this question, we compared the levels of citrullinated proteins in frontal cortex between patients with sporadic CJD and AD. But we could not find significant differences of accumulation levels of citrullinated proteins in this region using Western blot analysis with anti-modified citrulline antibody (data not shown). Although we could not test various other neurodegenerative diseases, this result suggests the possibility that citrullination may reflect glial cell activation and result in a common phenomenon in many neurodegenerative diseases. Nevertheless, more detailed study of PAD and citrullination between CJD and other neurodegenerative conditions as well as the development of specific antibody against each of the newly identified citrullinated proteins may contribute to our understanding of citrullination-related pathogenesis of neurodegenerative diseases.

It is not clear why PADs, especially PAD2, is activated and upregulated in neurodegenerative conditions. In MS, the inflammatory cytokine tumor necrosis factor alpha (TNF-α) induces PAD4 nuclear translocation, in which histone H3 is hypercitrullinated and apoptosis of oligodendrocytes is induced [36]. In addition, PAD2 transgenic mice showed astrocytes and macrophage activation, and increased production of TNF-α [40]. In studies including our previous work and others [30, 33], upregulation of inflammatory cytokines such as interleukin 1α (IL-1α), IL-1β and TNF-α in the brains of experimental scrapie and CJD mice correlated with the onset and progression of clinical disease. Thus, it is possible that the induction of the proinflammatory cytokines during the progression of prion disease may activate and upregulate PAD enzymes.

The presence of PrP^{Sc} is a marker of prion pathogenesis and can be used as a diagnostic marker, but it is only useful for biopsy- or autopsy-derived brain samples. Accordingly, many researchers have tried to find useful diagnostic factors in brain, cerebrospinal fluid, blood, and urine, and various molecules have been suggested, such as PrP^{Sc}, 14-3-3 family, tau, alpha1-antichymotrypsin, and neuron-specific enolase [9, 15, 22, 26, 55]. In a recent report, in vitro deimination of ovine PrP showed PrP^{Sc}-like characteristics, such as an increase of beta-sheet structure and PK-resistant form [64]. Further characterization of newly identified citrullinated proteins that were identified in this study and other citrullinated proteins found in body fluids might provide markers for the pre-clinical phase of prion diseases.

In summary, citrullinated proteins and increased PAD2 were observed in brains of sCJD patients; by immunohistochemistry, these proteins were found predominately in reactive astrocytes. The level of enzymatic activity of brain-derived PAD from sCJD patients was increased significantly compared to non-CJD controls. Finally, we suggest that the increased protein citrullination by activated PAD could be involved in the pathogenesis of prion diseases and may be an aid in the postmortem classification of human prion diseases.

Acknowledgments This study was supported by a grant of the Korea Healthcare technology R&D Project, Ministry for Health, Welfare and Family Affairs, Republic of Korea (A085082).

References

1. Aguzzi A, Sigurdson C, Heikenwaelder M (2008) Molecular mechanisms of prion pathogenesis. Annu Rev Pathol 3:11–40
2. Arita K, Hashimoto H, Shimizu T, Nakashima K, Yamada M, Sato M (2004) Structural basis for Ca(2+)-induced activation of human PAD4. Nat Struct Mol Biol 11:777–783
3. Aronica E, Yankaya B, Jansen GH et al (2001) Ionotropic and metabotropic glutamate receptor protein expression in glioneuronal tumours from patients with intractable epilepsy. Neuropathol Appl Neurobiol 27:223–237
4. Asaga H, Akiyama K, Ohsawa T, Ishigami A (2002) Increased and type II-specific expression of peptidylarginine deiminase in activated microglia but not hyperplastic astrocytes following kainic acid-evoked neurodegeneration in the rat brain. Neurosci Lett 326:129–132
5. Asaga H, Ishigami A (2001) Protein deimination in the rat brain after kainate administration: citrulline-containing proteins as a novel marker of neurodegeneration. Neurosci Lett 299:5–8
6. Bhattacharya SK, Bhat MB, Takahara H (2006) Modulation of peptidyl arginine deiminase 2 and implication for neurodegeneration. Curr Eye Res 31:1063–1071
7. Bhattacharya SK, Crabb JS, Bonilha VL, Gu X, Takahara H, Crabb JW (2006) Proteomics implicates peptidyl arginine deiminase 2 and optic nerve citrullination in glaucoma pathogenesis. Invest Ophthalmol Vis Sci 47:2508–2514
8. Brown AM, Ransom BR (2007) Astrocyte glycogen and brain energy metabolism. Glia 55:1263–1271
9. Castilla J, Saá P, Soto C (2005) Detection of prions in blood. Nat Med 11:982–985
10. Chang X, Han J (2006) Expression of peptidylarginine deiminase type 4 (PAD4) in various tumors. Mol Carcinog 45:183–196
11. Chang X, Han J, Pang L, Zhao Y, Yang Y, Shen Z (2009) Increased PADI4 expression in blood and tissues of patients with malignant tumors. BMC Cancer 9:40
12. Cornell-Bell AH, Finkbeiner SM, Cooper MS, Smith SJ (1990) Glutamate induces calcium waves in cultured astrocytes: long-range glial signaling. Science 247:470–473
13. DeArmond SJ, Fajardo M, Naughton SA, Eng LF (1983) Degradation of glial fibrillary acidic protein by a calcium dependent proteinase: an electroblot study. Brain Res 262:275–282
14. Eddleston M, Mucke L (1993) Molecular profile of reactive astrocytes—implications for their role in neurologic disease. Neuroscience 54:15–36
15. Evers S, Droste DW, Lüdemann P, Oberwittler C (1998) Early elevation of cerebrospinal fluid neuron-specific enolase in Creutzfeldt-Jakob disease. J Neurol 245:52–53
16. Fiacco TA, McCarthy KD (2006) Astrocyte calcium elevations: properties, propagation, and effects on brain signaling. Glia 54:676–690

17. Freixes M, Rodríguez A, Dalfó E, Ferrer I (2006) Oxidation, glycoxidation, lipoxidation, nitration, and responses to oxidative stress in the cerebral cortex in Creutzfeldt-Jakob disease. Neurobiol Aging 27:1807–1815
18. Gottlieb M, Matute C (1997) Expression of ionotropic glutamate receptor subunits in glial cells of the hippocampal CA1 area following transient forebrain ischemia. J Cereb Blood Flow Metab 17:290–300
19. Gray BC, Skipp P, O'Connor VM, Perry VH (2006) Increased expression of glial fibrillary acidic protein fragments and mucalpain activation within the hippocampus of prion-infected mice. Biochem Soc Trans 34:51–54
20. Guentchev M, Voigtländer T, Haberler C, Groschup MH, Budka H (2000) Evidence for oxidative stress in experimental prion disease. Neurobiol Dis 7:270–273
21. Hernandez MR, Agapova OA, Yang P, Salvador-Silva M, Ricard CS, Aoi S (2002) Differential gene expression in astrocytes from human normal and glaucomatous optic nerve head analyzed by cDNA microarray. Glia 38:45–64
22. Hsich G, Kenney K, Gibbs CJ, Lee KH, Harrington MG (1996) The 14-3-3 brain protein in cerebrospinal fluid as a marker for transmissible spongiform encephalopathies. N Engl J Med 335:924–930
23. Imboden JB (2009) The immunopathogenesis of rheumatoid arthritis. Annu Rev Pathol 4:417–434
24. Ishigami A, Ohsawa T, Hiratsuka M et al (2005) Abnormal accumulation of citrullinated proteins catalyzed by peptidylarginine deiminase in hippocampal extracts from patients with Alzheimer's disease. J Neurosci Res 80:120–128
25. Jang B, Kim E, Choi JK et al (2008) Accumulation of citrullinated proteins by up-regulated peptidylarginine deiminase 2 in brains of scrapie-infected mice: a possible role in pathogenesis. Am J Pathol 173:1129–1142
26. Jimi T, Wakayama Y, Shibuya S et al (1992) High levels of nervous system-specific proteins in cerebrospinal fluid in patients with early stage Creutzfeldt-Jakob disease. Clin Chim Acta 211:37–46
27. Jin JK, Choi JK, Lee HG, Kim YS, Carp RI, Choi EK (1999) Increased expression of CaM kinase II alpha in the brains of scrapie-infected mice. Neurosci Lett 273:37–40
28. Johnston AR, Black C, Fraser J, MacLeod N (1997) Scrapie infection alters the membrane and synaptic properties of mouse hippocampal CA1 pyramidal neurones. J Physiol 500:1–15
29. Kascsak RJ, Rubenstein R, Merz PA et al (1987) Mouse polyclonal and monoclonal antibody to scrapie-associated fibril proteins. J Virol 61:3688–3693
30. Kim JI, Ju WK, Choi JH et al (1999) Expression of cytokine genes and increased nuclear factor-kappa B activity in the brains of scrapie-infected mice. Mol Brain Res 73:17–27
31. Kizawa K, Takahara H, Troxler H, Kleinert P, Mochida U, Heizmann CW (2008) Specific citrullination causes assembly of a globular S100A3 homotetramer: a putative Ca2+ modulator matures human hair cuticle. J Biol Chem 283:5004–5013
32. Klareskog L, Rönnelid J, Lundberg K, Padyukov L, Alfredsson L (2008) Immunity to citrullinated proteins in rheumatoid arthritis. Annu Rev Immunol 26:651–675
33. Kordek R, Nerurkar VR, Liberski PP et al (1996) Heightened expression of tumor necrosis factor a, interleukin 1a, and glial fibrillary acidic protein in experimental Creutzfeldt-Jakob disease in mice. Proc Natl Acad Sci USA 93:9754–9758
34. Ladogana A, Puopolo M, Croes EA et al (2005) Mortality from Creutzfeldt-Jakob disease and related disorders in Europe, Australia, and Canada. Neurology 64:1586–1591
35. Loos T, Mortier A, Gouwy M et al (2008) Citrullination of CXCL10 and CXCL11 by peptidylarginine deiminase: a naturally occurring posttranslational modification of chemokines and new dimension of immunoregulation. Blood 112:2648–2656
36. Mastronardi FG, Wood DD, Mei J et al (2006) Increased citrullination of histone H3 in multiple sclerosis brain and animal models of demyelination: a role for tumor necrosis factor-induced peptidylarginine deiminase 4 translocation. J Neurosci 26:11387–11396
37. Méchin MC, Sebbag M, Arnaud J et al (2007) Update on peptidylarginine deiminases and deimination in skin physiology and severe human diseases. Int J Cosmet Sci 29:147–168
38. Moscarello MA, Mastronardi FG, Wood DD (2007) The role of citrullinated proteins suggests a novel mechanism in the pathogenesis of multiple sclerosis. Neurochem Res 32:251–256
39. Mouser PE, Head E, Ha KH, Rohn TT (2006) Caspase-mediated cleavage of glial fibrillary acidic protein within degenerating astrocytes of the Alzheimer's disease brain. Am J Pathol 168:936–946
40. Musse AA, Li Z, Ackerley CA et al (2008) Peptidylarginine deiminase 2 (PAD2) overexpression in transgenic mice leads to myelin loss in the central nervous system. Dis Model Mech 1:229–240
41. Nakashima K, Hagiwara T, Yamada M (2002) Nuclear localization of peptidylarginine deiminase V and histone deimination in granulocytes. J Biol Chem 277:49562–49568
42. Nicholas AP, King JL, Sambandam T et al (2003) Immunohistochemical localization of citrullinated proteins in adult rat brain. J Comp Neurol 459:251–266
43. Nicholas AP, Sambandam T, Echols JD, Tourtellotte WW (2004) Increased citrullinated glial fibrillary acidic protein in secondary progressive multiple sclerosis. J Comp Neurol 473:128–136
44. Newcombe J, Woodroofe MN, Cuzner ML (1986) Distribution of glial fibrillary acidic protein in gliosed human white matter. J Neurochem 47:1713–1719
45. Otvos L Jr, Cudic M (2002) Post-translational modifications in prion proteins. Curr Protein Pept Sci 3:643–652
46. Pamplona R, Naudí A, Gavín R et al (2008) Increased oxidation, glycoxidation, and lipoxidation of brain proteins in prion disease. Free Radic Biol Med 45:1159–1166
47. Pekny M, Nilsson M (2005) Astrocyte activation and reactive gliosis. Glia 50:427–434
48. Peoc'h K, Manivet P, Beaudry P et al (2000) Identification of three novel mutations (E196K, V203I, E211Q) in the prion protein gene (PRNP) in inherited prion diseases with Creutzfeldt-Jakob disease phenotype. Hum Mutat 15:482
49. Pritzker LB, Joshi S, Gowan JJ, Harauz G, Moscarello MA (2000) Deimination of myelin basic protein. 1. Effect of deimination of arginyl residues of myelin basic protein on its structure and susceptibility to digestion by cathepsin D. Biochemistry 39:5374–5381
50. Proost P, Loos T, Mortier A et al (2008) Citrullination of CXCL8 by peptidylarginine deiminase alters receptor usage, prevents proteolysis, and dampens tissue inflammation. J Exp Med 205:2085–2097
51. Prusiner SB (1998) Prions. Proc Natl Acad Sci USA 95:13363–13383
52. Raijmakers R, Vogelzangs J, Raats J et al (2006) Experimental autoimmune encephalomyelitis induction in peptidylarginine deiminase 2 knockout mice. J Comp Neurol 498:217–226
53. Sandberg MK, Wallén P, Wikström MA, Kristensson K (2004) Scrapie-infected GT1-1 cells show impaired function of voltage-gated N-type calcium channels (Ca(v) 2.2) which is ameliorated by quinacrine treatment. Neurobiol Dis 15:143–151
54. Senshu T, Sato T, Inoue T, Akiyama K, Asaga H (1992) Detection of citrulline residues in deiminated proteins on polyvinylidene difluoride membrane. Anal Biochem 203:94–100